Supporting Information

Triggering of Low-Valence Molybdenum in Multiphasic MoS_2 for Effective Reactive Oxygen Species (ROS) Output in Catalytic Fenton-like Reactions

Yu Chen,[a, b, c] Gong Zhang, [b] Qinghua Ji,[b] Huijuan Liu,[b] Jiuhui Qu [a, b]*

[a] Key Laboratory of Drinking Water Science and Technology Research Centre for Eco-Environmental Sciences, Chinese Academy of Sciences, Beijing 100085, China.

[b] Center for Water and Ecology, State Key Joint Laboratory of Environment Simulation and Pollution Control, School of Environment, Tsinghua University, Beijing 100084, China

[c] University of Chinese Academy of Sciences, Beijing 100049, China

*Corresponding Author: Email: jhqu@rcees.ac.cn

Text S1. The calculation method of Gibbs Free Energy.

The structural optimization and transition states have been calculated using DMol3 code. The generalized gradient approximation (GGA) with the Perdew–Burke–Ernzerhof (PBE) functional and all-electron double numerical basis set with polarized function (DNP) have been employed. The convergence tolerance of energy, maximum force and maximum displacement are 1.0×10^{-5} Ha, 2.0×10^{-3} Ha/Å and 5.0×10^{-3} Å (1Ha=27.21eV) for geometry optimization. The complete LST/QST search protocol, the SCF tolerance of 1.0×10^{-6} Ha and smearing of 0.005 Ha are set for transition states. The Grimme method for DFT-D correction is considered for all calculations. Each atom in the storage models is allowed to relax to the minimum in the enthalpy without any constraints.

Gibbs free energy change (ΔG) of each chemical reaction is calculated by:

$$\Delta G = \Delta E + \Delta ZPE - T\Delta S$$

where E, ZPE, T and S denote the calculated total energy, zero point energy, temperature and entropy, respectively.

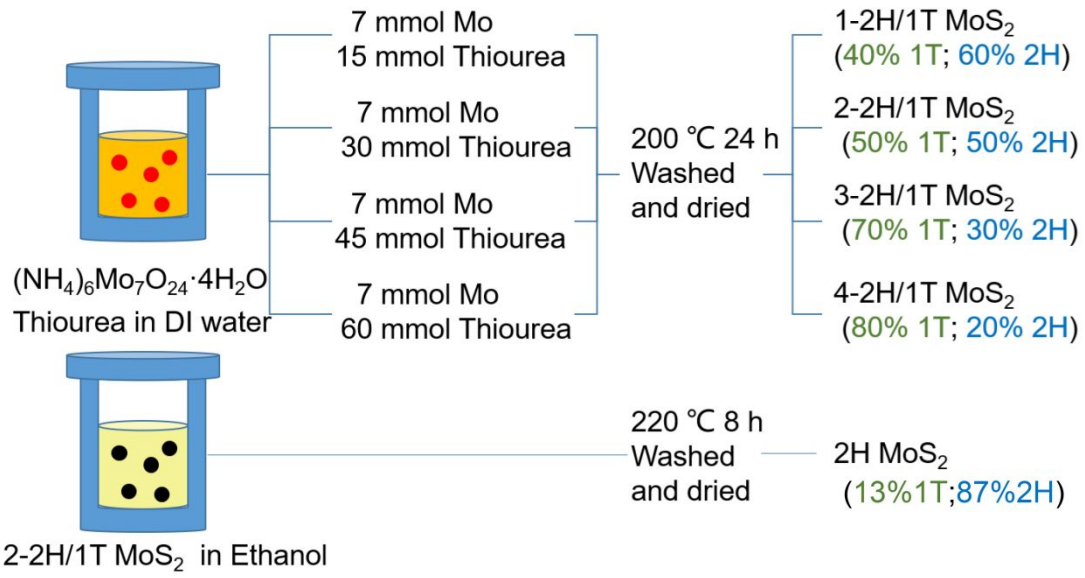

Figure S1. Schematic diagram of synthesize MoS_2. MoS_2 with various 1T phase concentration was synthesized by hydrothermal methods. **Chemicals**: $(NH_4)_6Mo_7O_{24}\cdot 4H_2O$ and thiourea (CH_4N_2S) were purchased from Aladdin Co. China. Nafion solutions (5% *wt*), 5,5-Dimethyl-1-pyrroline *N*-oxide (DMPO) and PMS ($KHSO_5\cdot 0.5KHSO_4\cdot 0.5K_2SO_4$) were purchased from Sigma Aldrich Co. Ethanol (EtOH), *tert*-butyl alcohol (TBA) and *iso*-propyl alcohol (IPA) were purchased from Beijing J&K Co. Ltd., China.

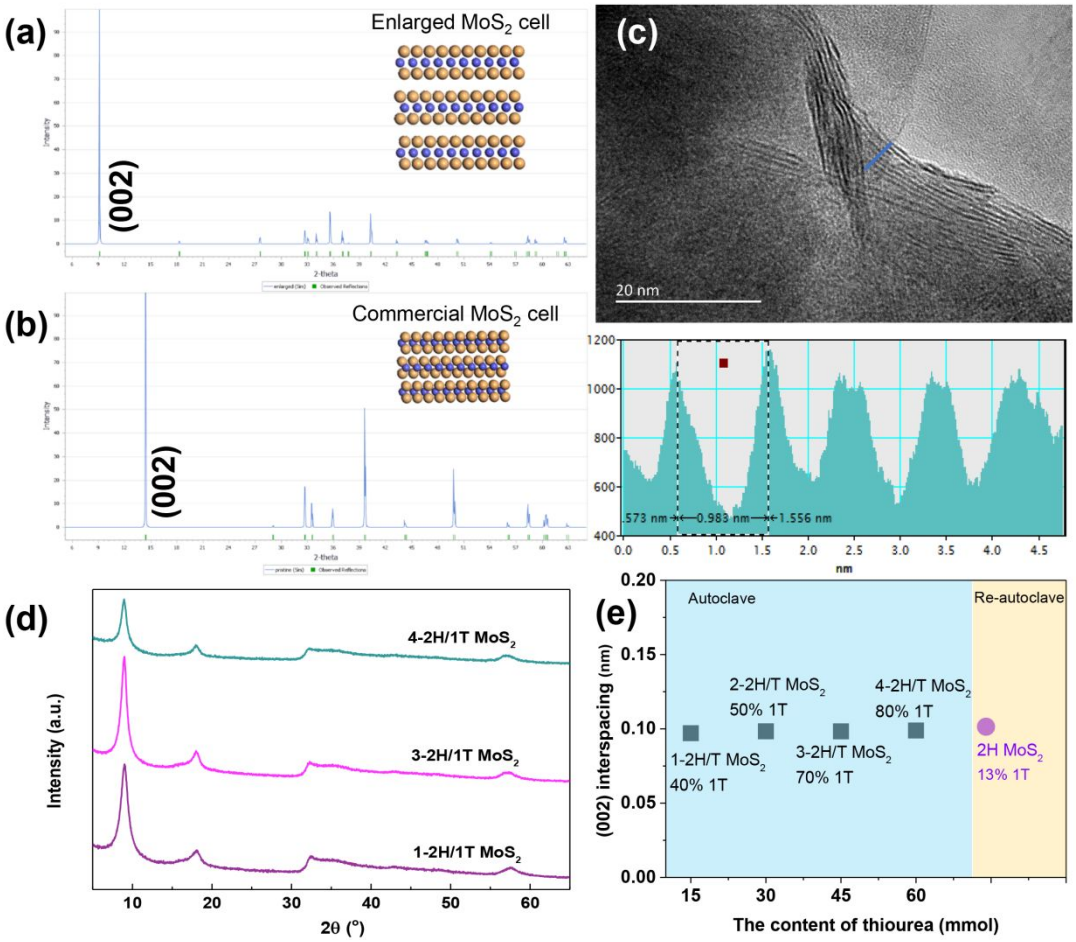

Figure S2. The XRD patterns of (a) enlarged MoS_2 cell and (b) pristine MoS_2 cell, (c) The cross-sectional TEM image and corresponding layer distance of 2-2H/1T MoS_2, (d) XRD patterns of 1-2H/1T, 3-2H/1T and 4-2H/1T MoS_2, (e) the relationship between concentration of thiourea and (002) interspacing.

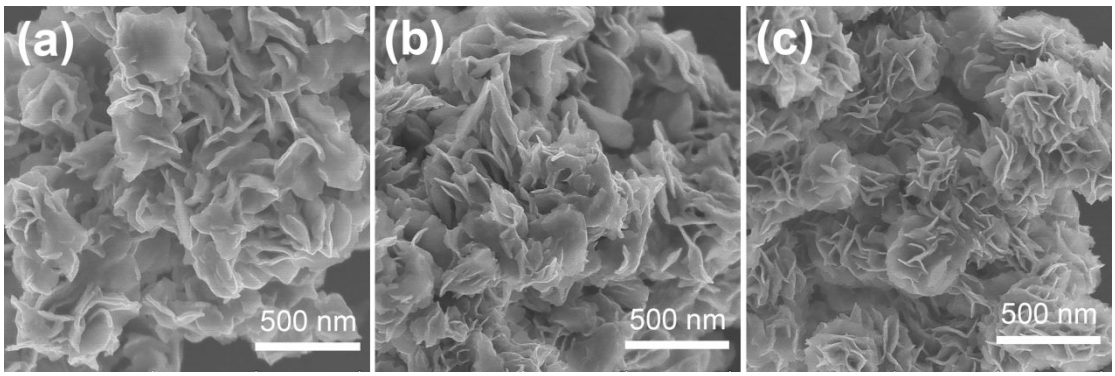

Figure S3. FESEM images of (a) 1-2H/1T MoS_2, (b) 3-2H/1T MoS_2 and (c) 4-2H/1T MoS_2.

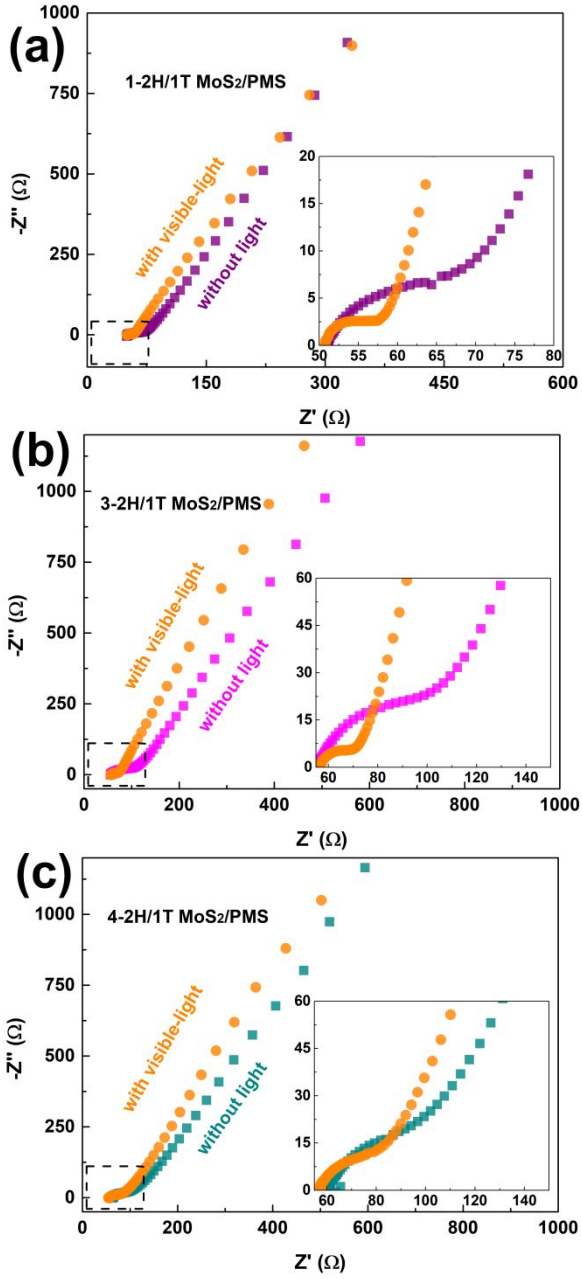

Figure S4. Nyquist plots of the (a) 1-2H/1T MoS_2, (b) 3-2H/1T MoS_2 and (c) 4-2H/1T MoS_2 electrode measured in a solution of 0.5 mM PMS and 0.1 M $NaSO_4$ over the frequency range from 10^5 Hz to 10^{-2} Hz. The inset shows the magnified EIS at high frequency.

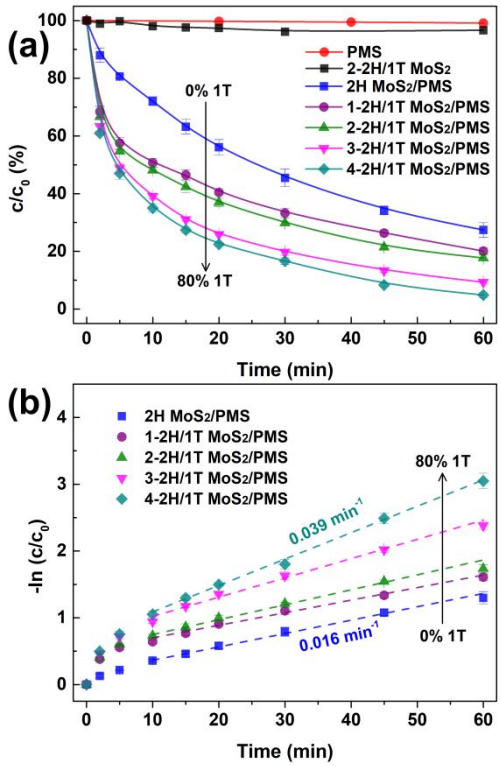

Figure S5. (a) Removal efficiency of 2,4-D using MoS_2 under activation of PMS, (b) pseudo-first-order kinetics regression in selected processes. Reaction conditions: $[2,4\text{-}D]_0$= 25 μM; $[PMS]_0$= 0.5 mM; Catalyst dosage= 100 mg·L^{-1}, initial pH= 5.0, Temperature= 20 °C.

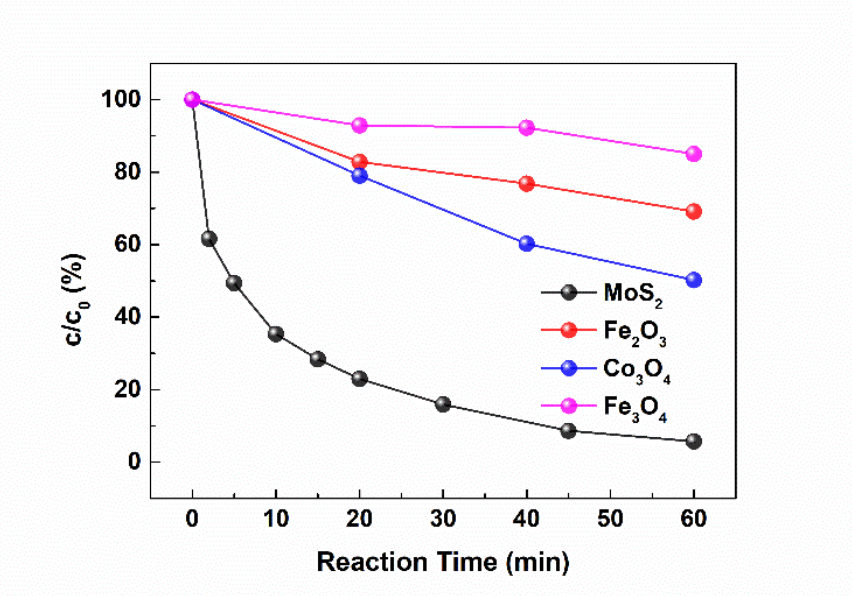

Figure S6. The evaluation of catalytic PMS performance using 4-2H/1T MoS_2 and benchmarks (Fe_2O_3, Fe_3O_4, Co_3O_4). The benchmarks were all purchased from Sino pharm Co. Ltd. Shanghai.

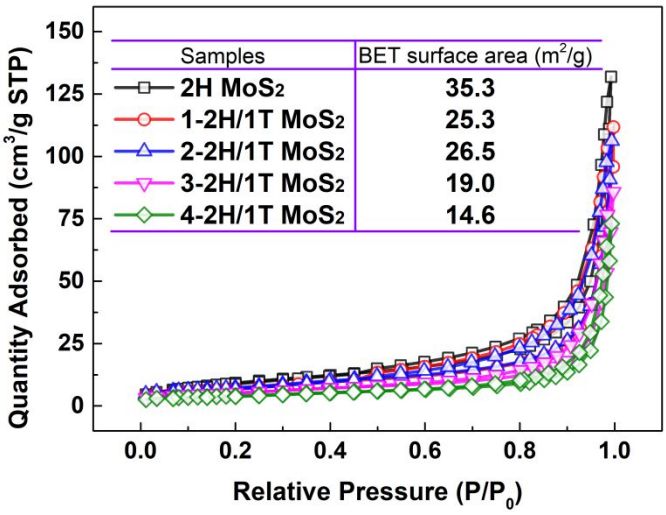

Figure S7. The BET surface area of 2H, 1-2H/1T, 2-2H/1T, 3-2H/1T and 4-2H/1T MoS_2 samples.

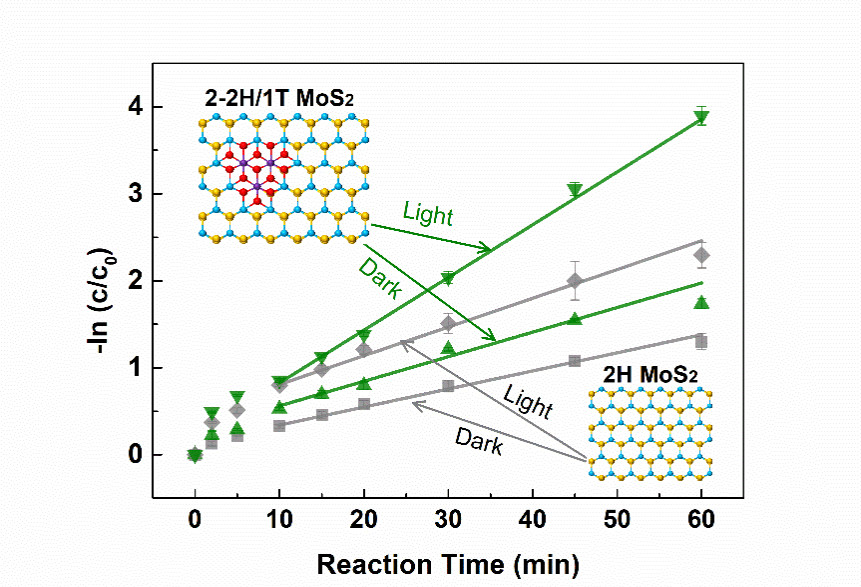

Figure S8. Pseudo-first-order kinetic fitting on 2,4-D degradation in 2H MoS_2/PMS or 2-2H/1T MoS_2/PMS system.

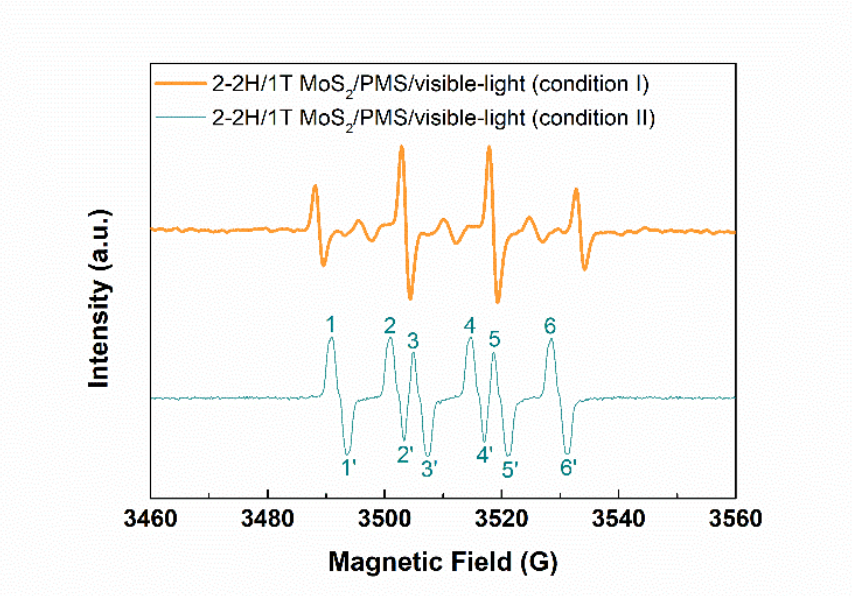

Figure S9. EPR spectra recorded in 2-2H/1T MoS_2/PMS/visible-light system.

Condition I: $[2,4\text{-D}]_0$= 25 μM; $[PMS]_0$= 0.5 mM; MoS_2 dosage= 100 $mg \cdot L^{-1}$, initial pH= 5.0, Temperature= 20 °C

Condition II: $[2,4\text{-D}]_0$= 25 μM; $[PMS]_0$= 50 mM; MoS_2 dosage= 1000 $mg \cdot L^{-1}$, initial pH= 5.0, Temperature= 20 °C

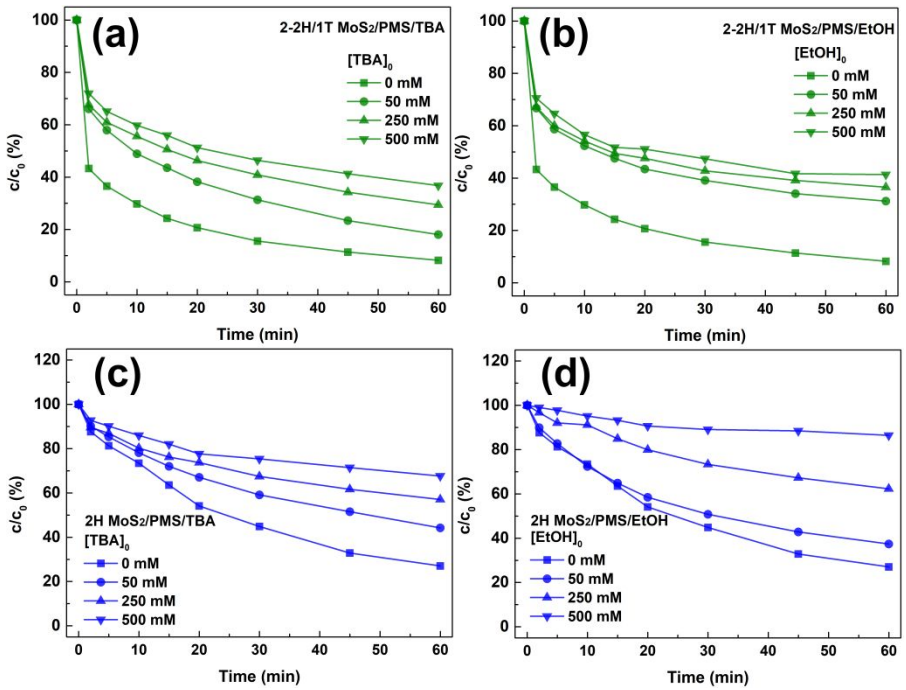

Figure S10. The 2,4-D degradations with radical scavengers in (a, b) 2-2H/1T MoS_2/PMS, (c, d) 2H MoS_2/PMS systems. Reaction conditions: $[2,4\text{-D}]_0$= 25 μM; $[PMS]_0$= 0.5 mM; MoS_2 dosage= 100 mg·L^{-1}, initial pH= 5.0, Temperature= 20 °C.

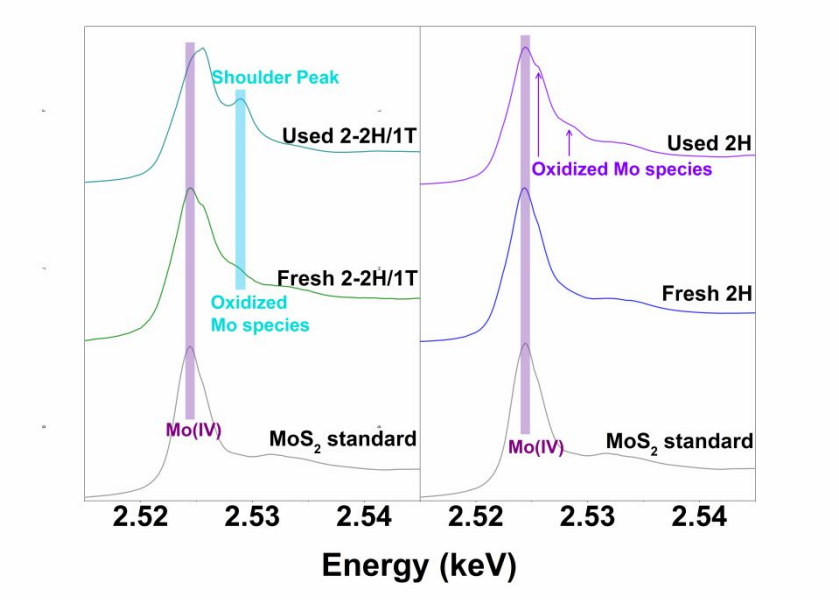

Figure S11. The Mo L_3-edge XANES data for 2H or 2-2H/1T MoS_2 samples before and after photo-catalytic PMS reactions.

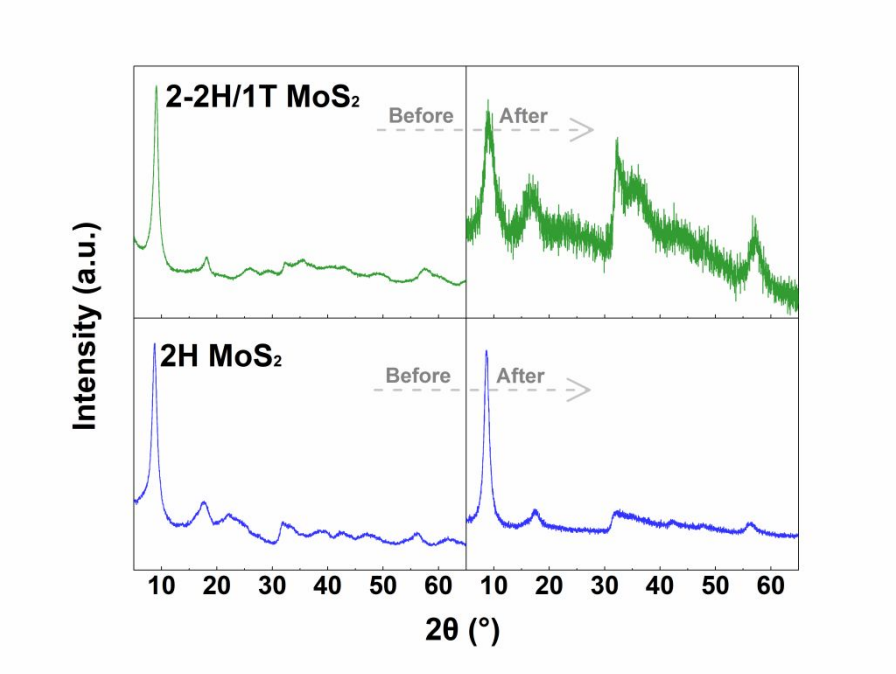

Figure S12. XRD patterns of 2-2H/1T MoS_2 and 2H MoS_2 after reactions.

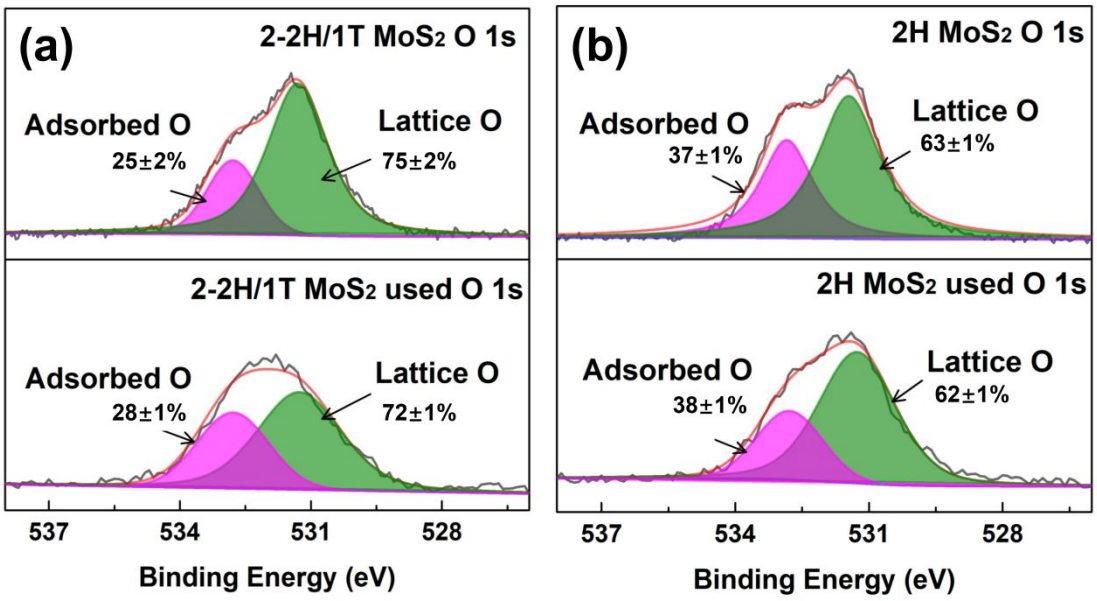

Figure S13. High-resolution XPS spectra of (a) O 1s for 2-2H/1T MoS_2 before and after 5 runs of reactions under visible-light irradiation, and (b) O 1s for 2H MoS_2 before and after 5 runs of reactions under visible-light irradiation.

Table S1. The phase distribution of various MoS_2 samples based on the deconvolution of Mo 3d

Samples	Mo $3d_{3/2}$		Mo $3d_{5/2}$		Phase distribution
	2H area	1T area	2H area	1T area	
2H MoS_2	7473	0	9484	0	13%±2% 1T
1-2H/1T MoS_2	11191	9545	15531	9312	40%±2% 1T
2-2H/1T MoS_2	5091	7002	7570	7185	50%±3% 1T
3-2H/1T MoS_2	3069	7105	4023	8392	70%±4% 1T
4-2H/1T MoS_2	942	2950	855	3717	80%±3% 1T

Table S2. Comparison of different catalysts for PMS activation in 2,4-D removal. (υ-value= $\frac{1}{m_{cat}}\frac{dn}{dt}$)

Catalyst (dosage: g L^{-1})	PMS dosage (g L^{-1})	Pollutants (mg L^{-1})	Removal (%)	*υ*-value* (μmol s^{-1} g_{cat}^{-1})	Reference
FeS (0.15)	0.3 (PS)	2,4-D (10 mg L^{-1})	100% (120 min)	0.042	1
HNPs (0.5)	0.9	2,4-D (5 mg L^{-1})	100% (40 min)	0.019	2
MCFNs (0.2)	0.6 (PMS) +16 ppm O_3	2,4-D (20 mg L^{-1})	100% (60 min)	0.125	3
ZVI (0.4)	Pure O_2 bubbling	2,4-D (221 mg L^{-1})	100% (150 min)	0.006	4
Benchmark Fe_2O_3 (0.1)	0.15	2,4-D (5.5 mg L^{-1})	25% (60 min)	0.018	Benchmark
Benchmark Fe_3O_4 (0.1)	0.15	2,4-D (5.5 mg L^{-1})	6% (60 min)	0.004	Benchmark
Benchmark Co_3O_4 (0.1)	0.15	2,4-D (5.5 mg L^{-1})	49% (60 min)	0.036	Benchmark
4-2H/1T MoS_2 (0.1)	0.15	2,4-D (5.5 mg L^{-1})	96% (60 min)	0.070	This work

*υ-value= $\frac{1}{m_{cat}}\frac{dn}{dt}$, here m_{cat} represents for the mass of catalyst (g), n is μmol of 2,4-D removal and t is reaction time (s).[5]

Table S3. The corresponding fitting parameters of $-\ln(c/c_0)$ vs *t* of various MoS_2/PMS system.

Samples	Fitting Parameters of $-\ln(c/c_0)$ versus t of various MoS_2		
	Slope*	Intercept	R^2
2H MoS_2 (Dark)	0.0169	0.1738	0.99
2H MoS_2 (Light)	0.0303	0.3339	0.97
2-2H/1T MoS_2 (Dark)	0.0212	0.5551	0.99
2-2H/1T MoS_2 (Light)	0.0621	0.1978	0.99

*The second stage (10~60 min) was chosen to investigate reaction rate.

Supporting Information Reference

1. Chen, H.; Zhang, Z.; Feng, M.; Liu, W.; Wang, W.; Yang, Q.; Hu, Y., Degradation of 2,4-Dichlorophenoxyacetic Acid in Water by Persulfate Activated with FeS (Mackinawite). *Chem. Eng.J.* **2017,** *313*, 498-507.
2. Jaafarzadeh, N.; Ghanbari, F.; Ahmadi, M., Catalytic Degradation of 2,4-Dichlorophenoxyacetic acid (2,4-D) by Nano-Fe_2O_3 Activated Peroxymonosulfate: Influential Factors and Mechanism Determination. *Chemosphere* **2017,** *169*, 568-576.
3. Jaafarzadeh, N.; Ghanbari, F.; Ahmadi, M., Efficient Degradation of 2,4-Dichlorophenoxyacetic Acid by Peroxymonosulfate/Magnetic Copper Ferrite Nanoparticles/Ozone: A Novel Combination of Advanced Oxidation Processes. *Chem. Eng.J.* **2017,** *320*, 436-447.
4. Correia de Velosa, A.; Pupo Nogueira, R. F., 2,4-Dichlorophenoxyacetic acid (2,4-D) Degradation Promoted by Nanoparticulate Zerovalent Iron (nZVI) in Aerobic Suspensions. *J. Environ. Manage.* **2013,** *121*, 72-79.
5. Yang, D.; Feng, J.; Jiang, L.; Wu, X.; Sheng, L.; Jiang, Y.; Wei, T.; Fan, Z., Photocatalyst Interface Engineering: Spatially Confined Growth of $ZnFe_2O_4$ within Graphene Networks as Excellent Visible-Light-Driven Photocatalysts. *Adv. Funct. Mater.* **2015,** *25*, 7080-7087.